

On Transmission Node Structure in Interacting Systems

J. D. Barr* and C. A. Stafford

Department of Physics, University of Arizona, 1118 East Fourth Street, Tucson, AZ 85721

We provide a series of generic results regarding the structure of nodes in the retarded Green's function G of an interacting system, as exemplified by the extended Hubbard model. In particular: (1) due to an incompatibility between interactions of nearly any form and a precise definition of series propagation, degenerate geometric nodes are split or lifted by interactions; (2) degenerate nodes generically exist at the boundary between regimes of node splitting and node lifting and, in the presence of interactions, they require fine-tuning; (3) degenerate nodes are highly sensitive to perturbation and their sensitivity increases with their degeneracy. Moreover, for high degeneracies there is a tendency toward lifting rather than splitting.

We also propose a characterization of the node structure in extended Hubbard models at arbitrary filling in terms of either the eigenvalues of G , or equivalently, the roots of a polynomial. This shows that “Mott nodes” previously predicted to occur in the transmission spectra of molecular radicals¹ are fundamentally associated with nodes in the eigenvalues of the retarded Green's function that occur in open-shelled systems. This is accompanied by a low-energy two-pole approximation wherein each of the eigenvalues of G are mapped onto a Fermi-liquid-like renormalization of the Anderson model, for which the exact self-energy is provided.

I. INTRODUCTION

Absent interactions, the path integral formalism provides an intuitive relationship between the geometry of a quantum system and the interference effects exhibited by it. However, the nature of this correspondence in interacting systems is not obvious.

In this article we consider in particular nodes from destructive interference that arise in the retarded Green's function and consequently the transmission function associated with extended Hubbard models. Such models^{2–5} have been used to, for example, describe transport^{5–13} through molecular junctions and mesoscopic systems. In this context there is a great deal of experimental and theoretical evidence that most nodes present within noninteracting models persist in the presence of interactions.^{8,14–25}

However, in contrast to this, degenerate nodes present in interacting systems were previously observed to be split by Coulomb interactions within many-body calculations.^{26,27} Here we propose that the foregoing observation is the result of an inherent incompatibility between the presence of interactions and a definition of series propagation that can be formulated diagrammatically. Remarkably, we find violations of this definition cause large disruptions of degenerate nodes even when there are no interactions between the units arranged in series. The reason is fundamental: Amplitudes in interacting systems are not expressible as a sum of *geometric* Feynman paths. All possible field configuration *histories* contribute coherently to a propagator, and degenerate nodes are found to be strikingly sensitive to this (Figure 1).

We also show for the first time that degenerate nodes do exist in interacting systems. However, in light of the aforementioned breakdown of series propagation, we find that they generically require fine-tuning and that their sensitivity to perturbation and tuning increases

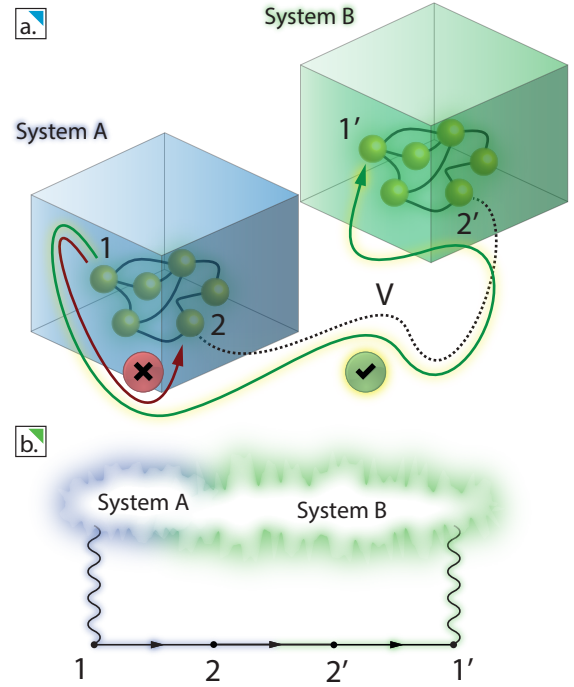


FIG. 1. (a) Two identical systems, A and B , linked by a matrix element V between orbitals 2 and $2'$. Even with interactions only *within* each system, a definition of series propagation is fundamentally broken by the processes depicted in (b). This can cause dramatic changes in the low-energy node structure of the propagator, e.g. permitting transport between 1 and $1'$ when it is forbidden between 1 and 2 .

with their order. Moreover, we provide the first reports that degenerate nodes can be lifted by interactions instead of split, that they generically lie at the boundary between regimes of splitting and lifting, that this splitting or lifting is an ill-conditioned function of parameters in the Hamiltonian, and that for high degeneracy there

is a tendency toward lifting.

To provide a simple conceptual framework for understanding the node structure in extended Hubbard models, we also develop a simple but remarkably accurate functional form for the eigenvalues of the low-energy retarded Green's function that qualitatively characterizes the node structure of the models we consider. It is reminiscent of two-pole approximations that have been applied to the Hubbard model,^{2,28} and it is found to be equivalent to mapping each eigenvalue of the retarded Green's function onto the Green's function of a Fermi-liquid-like²⁹ renormalization of the Anderson model.³⁰

Using this, we show that so-called “Mott nodes”, reported previously in theoretical predictions of molecular transmission spectra¹ and in the Hubbard model,³¹ are associated with nodes in the eigenvalues of the retarded Green's function in extended Hubbard models. We note that such nodes also appear at high energies, and identify them as being generically due to the interference of field configuration histories. In this context, “eigenvalue nodes” responsible for Mott nodes are interpreted as being due to the destructive interference of particle-like and hole-like processes mediated by the *same* single-particle orbital. This refines earlier work¹ advancing the interpretation that the Mott node itself is directly due to particle-hole interference, which, while true in the context previously considered, turns out to be a special case.

Finally, we also cast the nodes of the retarded Green's function as the roots of a polynomial, which provides a formal connection between the perturbation of nodes

and the perturbation of the coefficients of a polynomial. While this formalism gives the nodes of the Green's function exactly at all energies, we find it practical to develop a reduced-order polynomial that characterizes low-energy node structure. In this context, split and lifted degenerate nodes correspond respectively to the real and complex roots of this polynomial.

The organization of this article is as follows: In Section II we develop a definition of series propagation and remark briefly upon the connection between propagation in an isolated system and transmission through it. In Section III, we provide an overview of the relationship between the breakdown of this definition of series propagation and the disruption of degenerate nodes in the presence of Coulomb interactions. In Section IV, we describe a connection between electronic structure and node structure in extended Hubbard models that characterizes low-energy nodes in such systems at arbitrary filling. This is then used to provide insight into a few generic properties of the node structure in interacting systems.

Many of the results that are described in Sections III and IV are based upon a detailed series of case studies of nodes in simple extended Hubbard models. For the sake of clarity, these do not appear in the main text and instead have been organized in Appendix A. Similarly, the technical details regarding the connection between nodes in the transmission function and nodes in the retarded Green's function appear in Appendix B. Finally, a derivation of the two-pole approximation for the eigenvalues of the Green's function used in Section IV appears in Appendix C.

II. A DEFINITION OF SERIES PROPAGATION

Consider the system depicted in Figure 1 consisting of two interacting systems A and B linked by a single matrix-element V . For the sake of concreteness, we take an extended Hubbard model² with spin and particle-hole symmetry for the interactions, in which case the Hamiltonian of the composite system $A + B$ is of the form:

$$\begin{aligned} \mathcal{H}^{A+B} = & \underbrace{- \sum_{i,j,\sigma} H_{ij}^A d_{i\sigma}^\dagger d_{j\sigma} + \frac{1}{2} \sum_{i,j} U_{ij}^A \rho_i \rho_j}_{\text{System A}} \\ & \underbrace{- \sum_{i,j,\sigma} H_{ij}^B c_{i\sigma}^\dagger c_{j\sigma} + \frac{1}{2} \sum_{i,j} U_{ij}^B \eta_i \eta_j}_{\text{System B}} \\ & \underbrace{- \sum_{\sigma} (V c_{n\sigma}^\dagger d_{m\sigma} + \text{H.c.}) + \frac{1}{2} \sum_{i,j} U_{ij}^{AB} \rho_i \eta_j}_{\text{Coupling}} \end{aligned} \quad (1)$$

where $\rho_i = \sum_{\sigma} d_{i\sigma}^\dagger d_{i\sigma} - 1$ and $\eta_i = \sum_{\sigma} c_{i\sigma}^\dagger c_{i\sigma} - 1$. Here $c_{n\sigma}^\dagger$ and $d_{n\sigma}^\dagger$ respectively create electrons with spin σ on the n th site of systems A and B .

The amplitude for a particle added to the α th orbital of system A at time 0 to be observed in the β th orbital of system B at time t is proportional to a Green's function $G_{\beta\alpha}(t, 0) = -i\hbar\Theta(t)\langle d_\beta(t) d_\alpha^\dagger(0) \rangle$. We define series propagation in this context via the requirement that $G_{\beta\alpha}$ be expressible as a coherent sum over Feynman paths,³²

each corresponding to a process wherein a particle propagates back and forth through each system in series, eventually ending up in the β th orbital of system B . The most general expression for $G_{\beta\alpha}$ under these conditions is:

$$\begin{aligned}
G_{\beta\alpha}(t, 0) = & \underbrace{\int_0^t d\tau_1 G_{n\alpha}^A(\tau_1, 0) \Delta G_{\beta m}^B(t, \tau_1)}_{\text{Direct transmission}} \\
& + \underbrace{\int_0^t d\tau_1 \int_{\tau_1}^t d\tau_2 \int_{\tau_2}^t d\tau_3 G_{n\alpha}^A(\tau_1, 0) \Delta G_{mm}^B(\tau_2, \tau_1) \Delta^* G_{nn}^A(\tau_3, \tau_2) \Delta G_{\beta m}^B(t, \tau_3)}_{\text{Transmission mediated by reflections at times } \tau_1 \text{ and } \tau_2} \\
& + \dots
\end{aligned} \tag{2}$$

where Δ is an amplitude associated with hopping between A and B , and G^A and G^B are amplitudes associated with propagation within A and B . These do not need to be Green's function associated the *isolated* systems, though they can be. We merely assume all the amplitudes are causal in the sense that $G_{ij}(t, 0) = 0$ for $t < 0$.

In this case, time translation invariance implies:

$$\begin{aligned}
G_{\beta\alpha}(t, 0) = & \int_{-\infty}^{\infty} d\tau_1 G_{n\alpha}^A(\tau_1) \Delta G_{\beta m}^B(t - \tau_1) \\
& + \int_{-\infty}^{\infty} d\tau_1 d\tau_2 d\tau_3 G_{n\alpha}^A(\tau_1) \Delta G_{mm}^B(\tau_2 - \tau_1) \Delta^* G_{nn}^A(\tau_3 - \tau_2) \Delta G_{\beta m}^B(t - \tau_3) \\
& + \dots
\end{aligned} \tag{3}$$

which is a Dyson equation³³ with the self-energy $\Sigma_{ij}(\tau) = \Delta\delta(\tau)\delta_{in}\delta_{jm}$. Applying the convolution theorem then yields a geometric series in the energy domain:

$$\begin{aligned}
G_{\beta\alpha} &= G_{n\alpha}^A \Delta G_{\beta m}^B + G_{n\alpha}^A \Delta G_{mm}^B \Delta^* G_{nn}^A \Delta G_{\beta m}^B + \dots \\
&= \frac{G_{n\alpha}^A \Delta G_{\beta m}^B}{1 - G_{mm}^B \Delta^* G_{nn}^A \Delta} = \frac{G_{n\alpha}^A V G_{\beta m}^B}{1 - G_{nn}^A G_{mm}^B |V|^2}
\end{aligned} \tag{4}$$

The last equality follows from the condition that the hopping amplitude Δ , which has not been specified till now, is equal to V . This ensures that the foregoing definition gives the exact result for noninteracting systems, as the self-energy Σ above is then the tunneling self-energy¹² associated with V . For clarity, the energy dependence of the amplitudes G_{ij} is left as implicit.

We note here that, although the intuitive case of $G_{\beta\alpha}(t, 0) = -i\hbar\Theta(t)\langle d_\beta(t)d_\alpha^\dagger(0) \rangle$ was considered first to formulate our definition of series propagation, the preceding applies equally to the retarded Green's function from the Keldysh formalism:³⁴ $G_{\beta\alpha}(t, 0) = -i\hbar\Theta(t)\langle \{d_\beta(t), d_\alpha^\dagger(0)\} \rangle$. Transport related quantities are elegantly expressed via this quantity, as it combines the amplitudes for both particle-like and hole-like processes.^{11,12,35}

Thus, throughout the remainder of this work we consider only the retarded Green's function, though the preceding is not specific to it. The precise relationship between the retarded Green's function of a system and the associated elastic transmission function is given in Appendix B. We also note that when one of the systems is a set of metallic electrodes and bare Green's functions are taken for $G^{A,B}$, the definition presented here reduces to the so-called elastic cotunneling approximation that has been studied before.³⁶⁻³⁸

We now consider the relationship between this definition of series propagation and node structure in interacting systems.

III. TOPOLOGY AND NODE STRUCTURE: THE BREAKDOWN OF SERIES PROPAGATION

Eq. (4) implies that a node at energy E in $G_{n\alpha}^A$ is sufficient to cause a node at the same energy in $G_{\beta\alpha}$ provided $G_{\beta n}^B$ is bounded in the vicinity of E . Equivalently, within the foregoing formulation of series transmission, if a virtual particle with a given energy can not propagate from α to n , it can not propagate from α to β

by way of coupling between n and m . In particular, if $G_{n\alpha}^A$ and $G_{\beta m}^B$ both vanish according to a power law, i.e. $G \propto (E - E_0)^\eta$, then Eq. (4) implies the amplitude $G_{\alpha\beta}$ exhibits a degenerate node, vanishing as $(E - E_0)^{2\eta}$.

With interactions these properties do not hold because the foregoing definition of series propagation, and consequently Eq. (2), breaks down. This is true even absent interactions between systems A and B . In the case studies presented in section A, we find that *even when there*

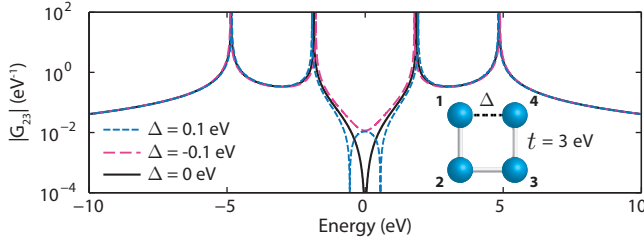


FIG. 2. The element G_{23} of the retarded Green's function for the depicted tight-binding model ($t_{12} = t_{23} = t_{34} \equiv t = 3$ eV, $t_{14} \equiv \Delta$). This system exhibits a degenerate node at $E = 0$ when $\Delta = 0$ eV (black), but for $\Delta = \pm 0.1$ eV the node is respectively lifted or split. Although in this case there are no interactions, we find that degenerate nodes generically sit at the boundary between node splitting and lifting.

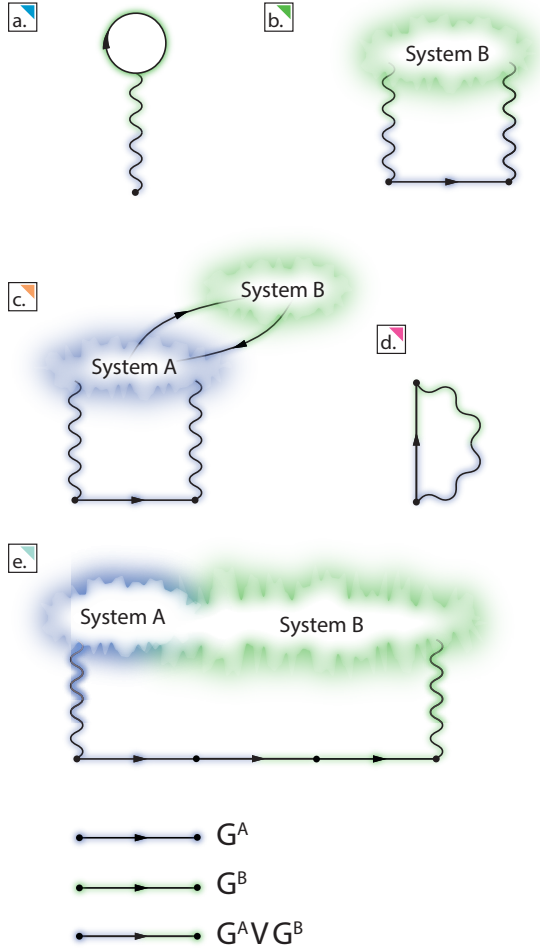
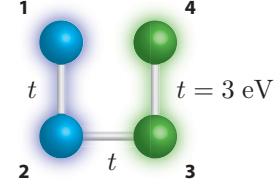


FIG. 3. Diagrams depicting processes that are inconsistent with a definition of pure series propagation between system A (blue) and system B (green). Diagrams (a) - (c) are consistent with a weak definition of series propagation, whereas (d) and (e) are not. We find the presence of either (d) or (e) destroys degenerate nodes otherwise expected on the basis of series propagation.



$$U_{nm} = \begin{cases} U_\gamma & \text{if } (n, m) = (1, 4) \text{ or } (n, m) = (4, 1) \\ 5 \text{ eV} & \text{otherwise} \end{cases}$$

FIG. 4. The geometry and extended Hubbard parameters associated with the interacting supernode depicted in Figure 5.

are no Coulomb interactions between the systems, and even when G^A and G^B are dressed exactly by the coupling of A to B, violations the foregoing definition of series propagation dramatically alter the structure of degenerate nodes at, for example, molecular energy scales. Ultimately, the reason is fundamental: Amplitudes in interacting systems are not expressible as a sum of *geometric* Feynman paths. All possible field configuration *histories* contribute coherently to a propagator. Thus, the factorization defined by Eq. (2) omits processes like those represented by the Feynman diagrams depicted in Figure 3:

Diagrams of class (a) and (b) are present only when there are long-ranged Coulomb interactions between A and B, and can be interpreted as dressing the Green's function in Eq. (2). Diagrams of class (c) can be viewed in the same manner but exist even absent intersystem interactions. The nonlocal exchange in (d) does require long-ranged Coulomb interactions, but can not be treated by dressing G^A . It is formally equivalent to introducing new matrix elements between A and B that alter their mutual connectivity. The final class (e) is inconsistent with series propagation in the purest sense – it exists generically, can not be treated within any formalism that involves only single-particle Green's functions for A and B, and does not arise from Coulomb interactions between the systems.

In the case studies presented in Appendix A, we find that for two identical systems arranged in series, the presence of diagrams of the form (d) or (e) is necessary and sufficient for the disruption of degenerate nodes that would otherwise be expected on the basis of series propagation. When present, diagrams of the form (d) usually correspond to self-energies that are quantitatively larger than those associated with the higher order diagrams (e). However, we find either (d) or (e) is capable of imparting very large changes to interference effects otherwise expected on the basis of series propagation. Under some circumstances, we find they compete and lead to novel node structure.

A curious example of this is furnished by an interacting supernode present in a four-site extended Hubbard

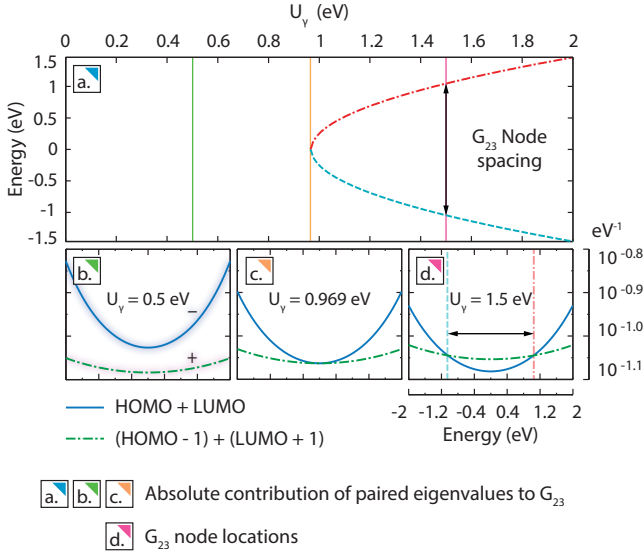


FIG. 5. The node locations (a) in a four-site extended Hubbard model presented in section A plotted as a function of an element U_γ of the interaction matrix. A degenerate node exists at $E = 0$ for a critical value ($U_\gamma \approx 0.969$) but is either split or lifted at other values. In the lifting regime, the eigenvalues of G corresponding to the HOMO and LUMO make the dominant contribution everywhere within the HOMO-LUMO gap (a-c). In the splitting regime, the dominant contribution is from the HOMO - 1 and LUMO + 1 eigenvalues in the region bracketed by the nodes (b-d).

model depicted in Figure 4, which is studied in more detail in Appendix A. In the present context the pertinent observation is that, while this system exhibits a higher-order node at the particle-hole symmetric point due to series propagation when there are no interactions, in the presence of Coulomb repulsion this feature is contingent upon the fine-tuning of an interaction matrix element. When this element deviates from a critical value, the degenerate node is rapidly split or lifted (Figure 5 panel a). In Appendix A, it is shown that the node lifting in this case is attributable to diagrams of the form (e) in Figure 3. More generally, we find that degenerate nodes generically lie at the boundary between the regimes of splitting and lifting.

Similar behavior can be observed in a noninteracting system wherein a degenerate node is either split or lifted depending upon the sign of a perturbation to a hopping matrix-element (Figure 2). Indeed, the splitting or lifting of the degenerate node discussed above can be interpreted in topological terms by considering an effective Hamiltonian defined by $\tilde{H} = H^{(1)} + \Sigma_0^C$. Here $H^{(1)}$ is the noninteracting part of the extended Hubbard Hamiltonian and Σ_0^C is the Coulomb self-energy evaluated at the node location $E = 0$. In this simple system, such a Hamiltonian accurately reproduces the Green's function at half-filling over a wide energy range that includes the HOMO-LUMO gap.

Moreover, in Appendix A it is shown that at the critical

tuning associated with the degenerate node in Figure 5, the (1,4) element of this Hamiltonian vanishes due to cancellation between nonlocal exchange and higher order processes. When this occurs \tilde{H} has the same topology as $H^{(1)}$, consistent with the existence of a degenerate node despite the presence of nontrivial Coulomb interactions between all the sites.

As a more general alternative to this topological interpretation, it is also possible to understand the crossover between node lifting and node splitting in terms of electronic structure. We pursue this in the next section, ultimately describing a simple model that can qualitatively explain the node structure at arbitrary filling in the extended Hubbard systems considered in this work.

IV. CONNECTING ELECTRONIC STRUCTURE WITH NODE STRUCTURE

The node structure of an interacting system can also be understood in terms of electronic structure. To this end, it is useful to consider the eigenvalues of the retarded Green's function G , which are analogous to transmission eigenvalues. In particular, the retarded Green's function of a system with no coupling to external degrees of freedom can be expressed exactly as:

$$G(E) = \sum_{\nu} \lambda_{\nu} |\nu\rangle \langle \nu| \quad (5)$$

where $|\nu\rangle$ is an energy-dependent normalized eigenvector of G and λ_{ν} is the corresponding eigenvalue. In Appendix C, it is shown that at zero temperature λ_{ν} is given exactly by an expression of the form:

$$\lambda_{\nu} = \sum_{\eta} \frac{Z_{\nu}^{\eta}}{E - \Delta E_{\eta} + i0^{+}} \quad (6)$$

Here the index η runs over all possible particle- and hole-like transitions out of occupied many-body ground states, and ΔE_{η} and Z_{ν}^{η} are corresponding transition energies and spectral weights.

In principle the number of terms in the sum above is huge—at least equal to the number of $N \pm 1$ particle many-body states, where N is the filling of the system. However, absent orbital degeneracy, at energies near the Fermi level each eigenvalue is given approximately by an expression of the form:

$$\lambda_{\nu}(E) \approx \frac{\tilde{Z}_{\nu}^p}{E - \tilde{\varepsilon}_{\nu}^p + i0^{+}} + \frac{\tilde{Z}_{\nu}^h}{E + \tilde{\varepsilon}_{\nu}^h + i0^{+}} \quad (7)$$

where $\tilde{\varepsilon}^{p,h}$ is an effective parameter that gives the energy cost of creating a particle or hole with state $|\nu\rangle$ and $\tilde{Z}_{\nu}^{p,h}$ is a corresponding spectral weight. This expression is developed in Appendix C and the justification for the use of effective parameters is considered carefully there. Here it suffices to note that we find this approximation to be remarkably accurate for the systems considered herein.

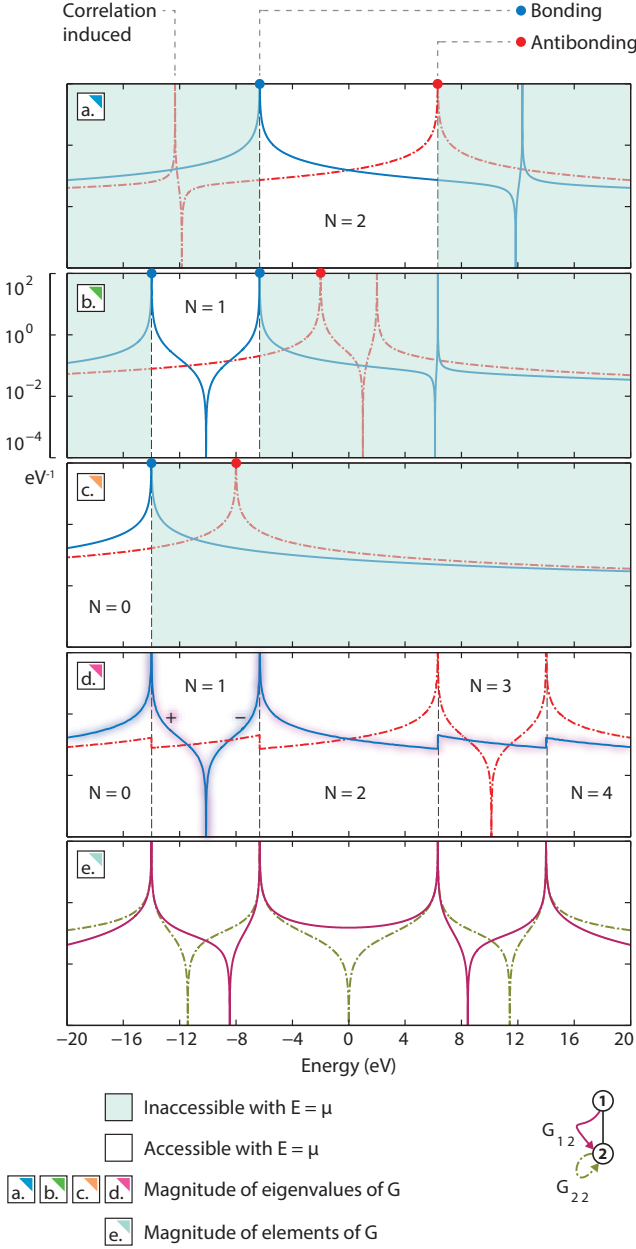


FIG. 6. Panels (a-d) depict the magnitude of the eigenvalues of the retarded Green's function for a symmetric two-site extended Hubbard model (system A). In (a), (b), and (c) the system is filled by two, one, and zero electrons respectively, whereas in panel (d) the Green's function is evaluated at the Fermi level. Panel (e) shows the the matrix-elements G_{nm} of the retarded Green's function, also evaluated at the Fermi level. Nodes in G_{nm} correspond to intersections of the eigenvalues in panel (d) above.

With long-ranged interactions, $\tilde{\varepsilon}^{p,h}$ can be approximated in terms of noninteracting energies and the charging energy of the system; similarly, $Z_\nu^p + Z_\nu^h \approx 1$.

Together Eq. (5) and Eq. (7) provide an essentially complete qualitative characterization of the low-energy node structure of a wide range of extended Hubbard mod-

els. This is demonstrated by way of example in Figure 6, which shows the exact eigenvalues of a symmetric two-site extended Hubbard model from Appendix A.

The approximation expressed by Eq. (7) corresponds primarily to neglecting the correlation-induced resonances at high energy (those in the shaded region), which are inaccessible to a particle propagating at the Fermi level. Due to the (anti)symmetry of the eigenvectors corresponding to the bonding and antibonding resonances, the nodes in an element of G occur where two of the eigenvalues are equal in magnitude. In more general cases the correspondence is modestly less intuitive, but the framework provided by Eq. (7) still characterizes the node structure accessible at the Fermi level, including the nodes in G_{nm} that occur at odd fillings on either side of the nodes in the eigenvalues.

In particular, in Appendix A it is shown that the nodes in G_{nm} in the $N = \pm 1$ filling regions occur due to a node in one of the eigenvalues λ_ν , and that their locations are dependent upon the node structure in the half-filling region. More generally, such nodes λ_ν occur in open-shelled systems. Like the correlation induced nodes at high energies, they are a signature of non-geometric destructive interference between field configuration histories.

More formally, Eq. (6) implies the energies of nodes in G_{nm} are given exactly by:

$$\sum_{\nu, \eta} \frac{A_\nu^\eta}{E - \Delta E_\eta + i0^+} = 0 \quad (8)$$

where $A_\nu = Z_\nu^\eta \langle n|\nu \rangle \langle \nu|m \rangle$ and η ranges over all transitions between many-body ground states and many-body states with an extra particle or hole. Putting the terms in this sum above over a common denominator yields the expression:

$$\sum_{\nu, \eta} A_\nu^\eta \prod_{\gamma \neq \nu} (E - \Delta E_\gamma) = 0 \quad (9)$$

where we have neglected infinitesimal imaginary terms.

The order of this polynomial is huge because it describes the location of all nodes, i.e. even those due to correlations at very high energies. Applying Eq. (7) renders it more intuitively useful, in which case we have:

$$\sum_{\substack{\nu \\ \{p,h\}}} \tilde{A}_\nu^{p,h} \prod_{\mu \neq \nu} (E - \tilde{\varepsilon}_\mu^{p,h}) = 0 \quad (10)$$

where both μ and ν range over single-particle eigenvectors. The degree of the polynomial is then at most $2(N-1)$, where N is the number of single-particle eigenstates. If we take into account the considerations in Appendix C, it can be seen that a polynomial of order $N-1$ suffices when the system is in a closed-shelled state. In practice, only a few of these roots are present at low-energies. Put another way, the number of nodes at low energy is at most half the number of eigenvalues competing in this region.

In light of the present discussion, the node structure depicted in Figure 5, explained topologically in the preceding section, can also be understood either in terms of the interference of the eigenvalues of G (panels a-c) or in terms of the roots of the polynomial in Eq. (10). In the former case the crossover between lifting and splitting occurs as the pair of eigenvalues making the dominant contribution to G near $E = 0$ switches from the HOMO and LUMO to the HOMO - 1 and the LUMO + 1. In the latter view, lifting occurs when Eq. (10) has complex roots whereas the splitting regime corresponds to real roots.

These equivalent perspectives generalize readily to the case of more complex systems, and imply that the node structure in similar models satisfies a few generic conditions: (1) *there is a strong tendency toward the preservation of the parity (i.e. evenness or oddness) of the number of nodes*; (2) *all degenerate nodes lie at the boundary between the regimes of node splitting and node lifting*; (3) *nodes in the eigenvalues of the Green's function occur in open-shelled states and at high energies due to non-geometric interference between field configuration histories and are responsible for the Mott nodes in G_{nm}* ; (4) *the sensitivity of a node to perturbation or the tuning of a parameter increases with its degeneracy*; (5) *the tendency of degenerate nodes to lift rather than split increases with their degeneracy*.

The last two points can be understood heuristically from the geometry of the eigenvalues λ_ν . Alternatively, they can be inferred formally based on Eq. (10) and well-known work³⁹ regarding the response of polynomial roots to the perturbation of their coefficients. In particular, the degenerate roots of a polynomial are an ill-conditioned function of its coefficients. The same work implies that even the location of nondegenerate nodes may in principle be an ill-conditioned function of parameters in the Hamiltonian, although this is expected to be a rare case.

These properties are exemplified by the extreme sensitivity of degenerate geometric nodes to any perturbation inconsistent with series propagation. For example, for two systems arranged in series that do not interact with each other but are themselves interacting, we find in Appendix A that processes fundamentally inconsistent with the notion of series propagation are sufficient to dramatically destroy degenerate nodes. Remarkably, in the same models these small deviations from pure series propagation have little effect on other low-energy features.

V. CONCLUSIONS

The retarded Green's function of an interacting system has the potential to exhibit rich and nontrivial node structure. However, in this work we have made a few generic observations: In extended Hubbard models (1) *there is a strong tendency toward the preservation of the parity (i.e. evenness or oddness) of the number of nodes*; (2) *degenerate nodes require fine-tuning in the*

presence of interactions and sit at the boundary between regimes of node splitting and node lifting; (3) *nodes in the eigenvalues of the Green's function occur in open-shelled states and at high energies due to non-geometric interference between field configuration histories*; (4) *the sensitivity of a degenerate node to the tuning of a parameter increases with its degeneracy*; and (5) *the tendency of degenerate nodes to lift upon perturbation rather than split increases with their degeneracy*.

These properties can be understood in terms of electronic structure by way of a simple approximation that qualitatively explains the node structure of the extended Hubbard models we considered, regardless of filling. More formally, nodes of the retarded Green's function are the roots of a polynomial. In some cases, node structure can also be understood in topological terms. However, in the presence of interactions, we find that geometric degenerate nodes predicted to exist on the basis of series propagation are present if and only if a definition of series propagation formulated herein is imposed artificially. This is true even when there are no interactions *between* the units arranged in series.

The reason for this is fundamental: Amplitudes in interacting systems are not expressible as a sum of *geometric* Feynman paths. All possible field configuration histories contribute coherently to an interacting propagator. Among the low energy interference features in interactions systems, degenerate nodes appear to be uniquely sensitive to this.

ACKNOWLEDGMENTS

This material is based upon work supported by the Department of Energy under Award Number de-sc0006699.

Appendix A: Case studies: Detailed analyses of the node structure in select extended Hubbard models

In the following we present detailed analyses of the node structure in select two and four site extended Hubbard models. We also touch briefly upon the node structure in larger systems. The material presented herein forms the basis for many of the observations made earlier in this work, but is necessarily more detailed and more technical than what has come before this point. The reader is encouraged to study the portions of interest to him or her.

Our starting point is Figure 7, which depicts a pair of two-site systems, A and B , joined by a single hopping matrix element V . The interactions are of the extended Hubbard form so that the full Hamiltonian is:

$$\mathcal{H}^{A+B} = \sum_{n,m,\sigma} H_{nm}^{(1)} d_{n\sigma}^\dagger d_{m\sigma} + \frac{1}{2} \sum_{nm} U_{nm} \rho_n \rho_m \quad (\text{A1})$$

where $\rho_n = \sum_\sigma d_n^\dagger d_n - 1$, which ensures particle-hole

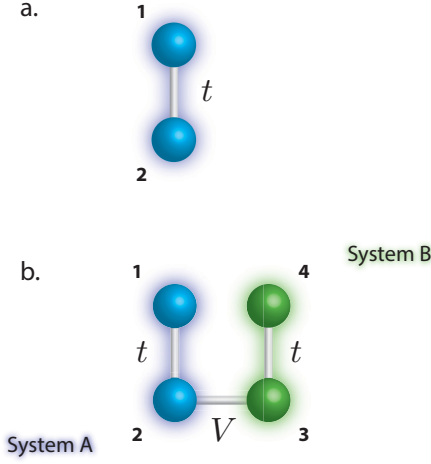


FIG. 7. Top (a): Two sites in an extended Hubbard model linked by a matrix element t . Bottom (b): Two systems of the form in (a) linked by a matrix element V and possibly with some Coulomb interactions between them. This is a realization of Figure 1 if we identify sites one and two as system A and sites three and four as system B.

symmetry, and:

$$H_{nm}^{(1)} = \begin{pmatrix} \mathbf{H}_A & \mathbf{H}_{AB} \\ \mathbf{H}_{AB}^\dagger & \mathbf{H}_B \end{pmatrix} = \begin{pmatrix} \epsilon & -t & 0 & 0 \\ -t^* & \epsilon & -V & 0 \\ 0 & -V^* & \epsilon & -t \\ 0 & 0 & -t^* & \epsilon \end{pmatrix}$$

$$U_{nm} = \begin{pmatrix} \mathbf{U}_A & \mathbf{U}_{AB} \\ \mathbf{U}_{AB}^\dagger & \mathbf{U}_B \end{pmatrix} = \begin{pmatrix} U & U_\alpha & U_\beta & U_\gamma \\ U_\alpha & U & U_\alpha & U_\beta \\ U_\beta & U_\alpha & U & U_\alpha \\ U_\gamma & U_\beta & U_\alpha & U \end{pmatrix}$$

This system has been studied as a model of a cross-conjugated molecule elsewhere,¹ but here we do not concern ourselves with detailed models of electronic structure that might obscure conceptual issues. Instead, we take a deliberately simple parameterization and tinker with it. In particular, we begin with:

$$\begin{aligned} \epsilon &= 0 \text{ eV}, & t &= 3 \text{ eV}, & U &= 10 \text{ eV}, & U_\alpha &= 6 \text{ eV}, \\ U_\beta &= 4 \text{ eV}, & V &= t, & U_\gamma &= U_\alpha \end{aligned} \quad (\text{A2})$$

This parameterization is roughly consistent with interactions that might be expected on the molecular scale,^{5,40,41} in particular for systems with a geometry respecting the symmetries of (b) in Figure 7.

1. Two sites (System A)

We first consider system A in isolation. The elements G_{nm} of the retarded Green's function in this case are plotted in Figure 6 panel (e) in the zero-temperature⁴²

limit but with the system maintained at a fixed chemical potential μ set equal to the energy E . Here, μ simply dictates the filling of the system. Panels (a-d) show the eigenvalues of the retarded Green's function either at fixed filling (a-c) or with the chemical potential equal to the energy (d). The shaded blue areas are the regions that are inaccessible to particles propagating at the Fermi level, i.e. the regions that do not contribute to linear response transport.^{35,43}

We now comment upon several noteworthy features in this figure:

a. The node in G_{22} at $E = 0$ eV: The noninteracting Green's function (not shown) exhibits a node at half-filling at $E = 0$. Formally, this is an antiresonance that occurs at the on-site potential of site one regardless of the matrix element t . Alternatively, it manifests as destructive interference between propagation mediated by the bonding and antibonding orbitals, i.e. the eigenstates of the Green's function with positive and negative parity respectively.

In panel (e) it is evident that this node persists in the interacting Green's function G_{22} . In fact, there is a simple symmetry argument that requires this: While in the interacting case there are no single-particle orbitals, the eigenvectors of G are still dictated entirely by symmetry and therefore identical to their noninteracting counterparts. In the present case, this observation is sufficient to imply that the node in g_{22} must also exist in G_{22} . Alternatively, this could be viewed as a consequence of the Luttinger theorem.^{1,44,45}

b. Singularities in the bonding and antibonding eigenvalues: In Appendix C, the eigenvalues λ_ν are given by the coherent sum of amplitudes associated with processes wherein a particle or hole is added to a many-body ground state. Absent interactions, each of these processes is simply the addition of a particle or hole to a noninteracting orbital, and the energy cost for corresponding particle-like and hole-like processes differs only in sign. Under these circumstances, the resonances for both kinds of processes occur at the same energy and there is one singularity per eigenvalue. With interactions this breaks down for two reasons: (1) When the system is charged (here, away from half filling) the energy cost of adding a particle to the system is no longer equal in magnitude to that of a hole; (2) transitions between ground states and correlated excited states lead to narrow resonances at high energies.

Reason (1) gives rise to Coulomb blockade^{46–49} in the context of transport, and occurs generically in presence of repulsive long-ranged interactions. It can be examined separately from (2) by taking $U_{nm} = U$, in which case the repulsive Coulomb energy depends only on the net charge of the system and the eigenvectors $\{|\nu\rangle\}$ are exactly equal to the noninteracting ones. In either cases (1) or (2), each singularity corresponds to some physical process wherein a particle or hole is added to the system in a manner that respects the symmetry of the corresponding eigenvector. This leads to novel node structure, as described below.

c. *The node in the bonding eigenvalue at $N = 1$ near $E = -10$ eV:* When $N = 1$ the bonding orbital is half-filled and thus accommodates both particle-like and hole-like addition. As noted above, in the presence of Coulomb interactions the resonances associated with these processes occur at distinct energies. Midway between them ($E \approx -10$ eV) the energy needed to create a virtual particle in this orbital is equal to that of a virtual hole, and so these processes contribute opposite amplitudes, completely suppressing propagation mediated by this orbital.

Note that the crucial fact here is not so much that the interference is between particle-like and hole-like propagation—this is formally responsible for nodes in G including the antiresonance in G_{22} —but that the destructive interference is between two *processes* with different amplitudes that are mediated by the *same* orbital.⁵⁰ This is totally alien to noninteracting systems and hence is beyond the scope of *geometric* Feynman paths, instead arising from the interference of field configuration histories. Nodes of this form are actually a general phenomenon that can be seen to arise between other singularities in the eigenvalues of G . Such nodes correspond to the coherent interference of histories (processes) involving states with the same symmetry. In a noninteracting system, they do not exist.

d. *The nodes in G_{nm} at $N = 1$ near $E = -10$ eV:* The aforementioned nodes in the eigenvalues of G are associated with nodes that occur in the elements of G around the same energy. Related nodes have been reported previously in the theoretical transmission spectrum of molecular radicals¹ and in the Hubbard model.³¹ In the present context, a node in the bonding eigenvalue can be seen around -10 eV in the $N = 1$ region. At this energy the positive parity eigenvector makes no contribution to the Green's function and G is perfectly antisymmetric, i.e. $G_{11} = -G_{12}$. This feature is bracketed by nodes in G_{11} and G_{12} that occur due to destructive interference between propagation through the bonding and antibonding resonances, i.e. at the locations where the magnitude of the eigenvalues intersect in panel (d). Between these nodes, propagation is mediated almost entirely by the antibonding resonance, despite the proximity of the bonding resonances.

Considering energies from left to right in the figure, as the bonding resonance is suppressed all the nodes in G_{nm} in the half-filling region reappear to the left of the node in the eigenvalue around -10 eV. As the bonding resonance opens back up, one node appears for each element of G that does *not* exhibit a node in the half-filling region. Thus the location of a node in G_{nm} at $N = 1$ is related to the existence or nonexistence of a node in the same element of G_{nm} at half-filling. An exceptional case is when the suppressed eigenvector is the only one that contributes to a particular element of the Green's function; in this situation the node in that element of G coincides with the node in the eigenvalue. Till now this is the only case that has been studied, but here we point

out that it is the exception rather than the rule. Overall, this behavior generalizes to larger systems, although the structure of the eigenvalues there is richer and can be complicated by, e.g., avoided crossings.

We now consider in a similar manner the node structure associated with the composite system $A + B$.

2. Four sites (System $A + B$)

We now consider the composite system depicted in Figure 7 (b) wherein system A is coupled to an identical system B by a matrix element V , forming a composite system $A + B$. The node spectrum in this case is depicted in Figure 8 in a manner analogous to Figure 6, which depicts the node structure of system A alone and is discussed at length in the foregoing section.

Most of the observations made there carry over to the case of the four-site system under consideration here. For example, the node structure at odd filling is related in the same way to nodes in the eigenvalues of the Green's function. However, for the remainder of this section we focus our attention on the case of half-filling. In particular, the node structure of G_{23} is noteworthy here:

Without interactions (not shown) the Green's function of system $A + B$ is given by Eq. (4). In this case, the node at $E = 0$ in G_{22} in system A and its counterpart in system B give rise to a degenerate node at $E = 0$ in system $A + B$ where $G_{23} \propto E^2$. However, as reported previously,²⁶ in the presence of interactions this is not the case. Instead, the degenerate node is split into two ordinary nodes which appear around ± 4 eV in panel (e) for the parameterization given by Eq. (A2). Since this is contrary to the predictions of Eq. (4), this node splitting is inconsistent with the definition of series propagation discussed earlier. It is thus attributable to some amalgam of the diagrams in Figure 3.

To shed light on what is happening, we use exact diagonalization to isolate several interesting combinations of these diagrams,⁵¹ as well as consider a variety of qualitatively interesting variations on the parameterization given by Eq. (A2). Along the way, we demonstrate results highlighted earlier in this work via a careful consideration of these cases. In particular, we show that the node splitting phenomenon just discussed occurs because degenerate nodes are extremely sensitive to the breakdown of series propagation, even when there are no interactions between systems A and B .

The cases considered are organized into the panels in Figure 9, which we now remark upon individually:

a. *Node structure with no diagrams from Figure 3:* By calculating the exact Green's functions of systems A and B in isolation and inserting these into Eq. (4), we may calculate the Green's function of system $A + B$ excluding precisely the diagrams depicted in Figure 3. This is equivalent to enforcing the strictest definition of series propagation proposed in section II, i.e. one wherein G^A and G^B in Eq. (4) are not dressed by the coupling

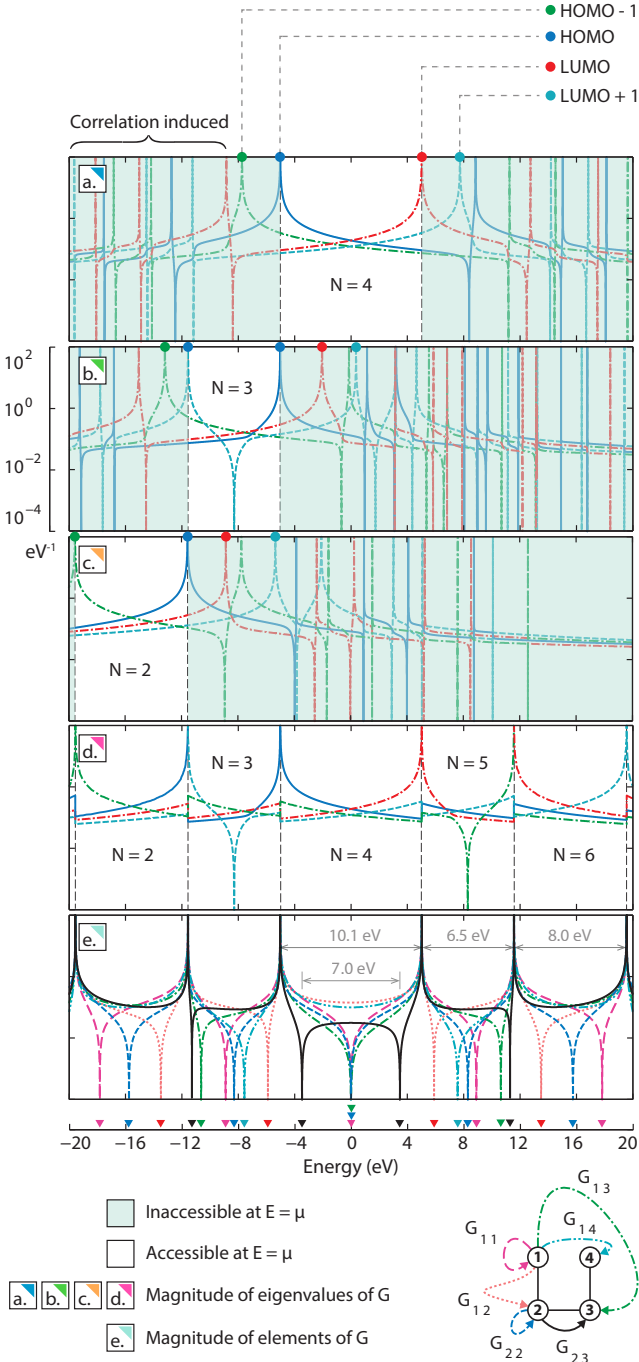


FIG. 8. Panels (a-d) depict the magnitude of the eigenvalues of the Green's function for system $A+B$ in a manner analogous to Figure 6. The associated eigenvectors (not shown) are now energy-dependent, but can still be classified based on symmetry. Panels (e) and (f) show the elements of the interacting and noninteracting Green's functions G_{nm} . The G_{23} element exhibits a pair of nodes that arise from the splitting of a degenerate node present in the absence of interactions. In the odd-filling regions a node in an eigenvalue of G causes clusters of nodes in G_{nm} .

of system A to system B .

The Green's function of $A+B$ calculated in this manner is shown in panel (a), and a degenerate node can be seen in G_{23} . This occurs because the elements G_{22}^A and G_{33}^B of the isolated Green's functions of A and B (not shown) exhibit nodes at $E=0$, and, with series propagation enforced, these necessarily give rise to a degenerate node in the composite system.

We now probe the effects of including one or more diagrams that are inconsistent with at least one of the definitions of series propagation considered earlier.

b. Node structure with diagrams of the form (a) + (b): A priori, (a) and (b) in Figure 3 are plausible candidates for the splitting of the degenerate node in G_{23} , and we can include these diagrams selectively via exact diagonalization. For combinations of (a) and (b) this entails calculating G^A and G^B including intersystem Coulomb interactions but with $V=0$. Inserting these into Eq. (4) then gives the desired Green's function, which is consistent with a weak definition of series propagation wherein $G^{A,B}$ are dressed to account for correlations caused by long-ranged Coulomb interactions between A and B .

The Green's functions $G^{A,B}$ calculated during this procedure (not shown) still exhibit nodes at $E=0$. Consequently, the the Green's function of $A+B$ calculated in this manner, which is depicted in panel (a), has a second order degenerate node. Thus, correlations induced by long-ranged Coulomb interactions between A and B are not responsible for splitting the degenerate node in this case.

c. Node structure with diagrams of the form (c): Diagrams of the form (c) can also be included selectively using exact diagonalization. To this end, the full Green's function of $A+B$ is first calculated without long-ranged Coulomb interactions but with $V \neq 0$. The corresponding Coulomb self-energy is then determined using the Dyson equation, and the parts of this associated with self-energies for systems A and B are extracted. These are used to determine the Green's functions $G^{A,B}$ dressed by the diagram shown, which are in turn used in Eq. (4).

The elements G_{22}^A and G_{33}^B of the dressed Green's functions of systems A and B that are obtained during this procedure (not shown) still exhibit nodes at $E=0$. Consequently, the degenerate node in the Green's function of system $A+B$ persists.

d. Node structure with diagrams of the form (a) - (c) Combinations of diagrams (a)-(c) may be selected for via exact diagonalization using almost the exact same procedure as for diagrams (c) alone. The only change necessary is to include long-range Coulomb interactions in the initial exact calculation of the Green's function of system $A+B$.

Again, the dressed Green's functions of A and B (not shown) possess nodes at $E=0$ that cause degenerate nodes in the Green's function for system $A+B$ when it is calculated using Eq. (4).

e. Node structure with diagrams of the form (a) + (d) (self-consistent Hartree-Fock): To probe the effects

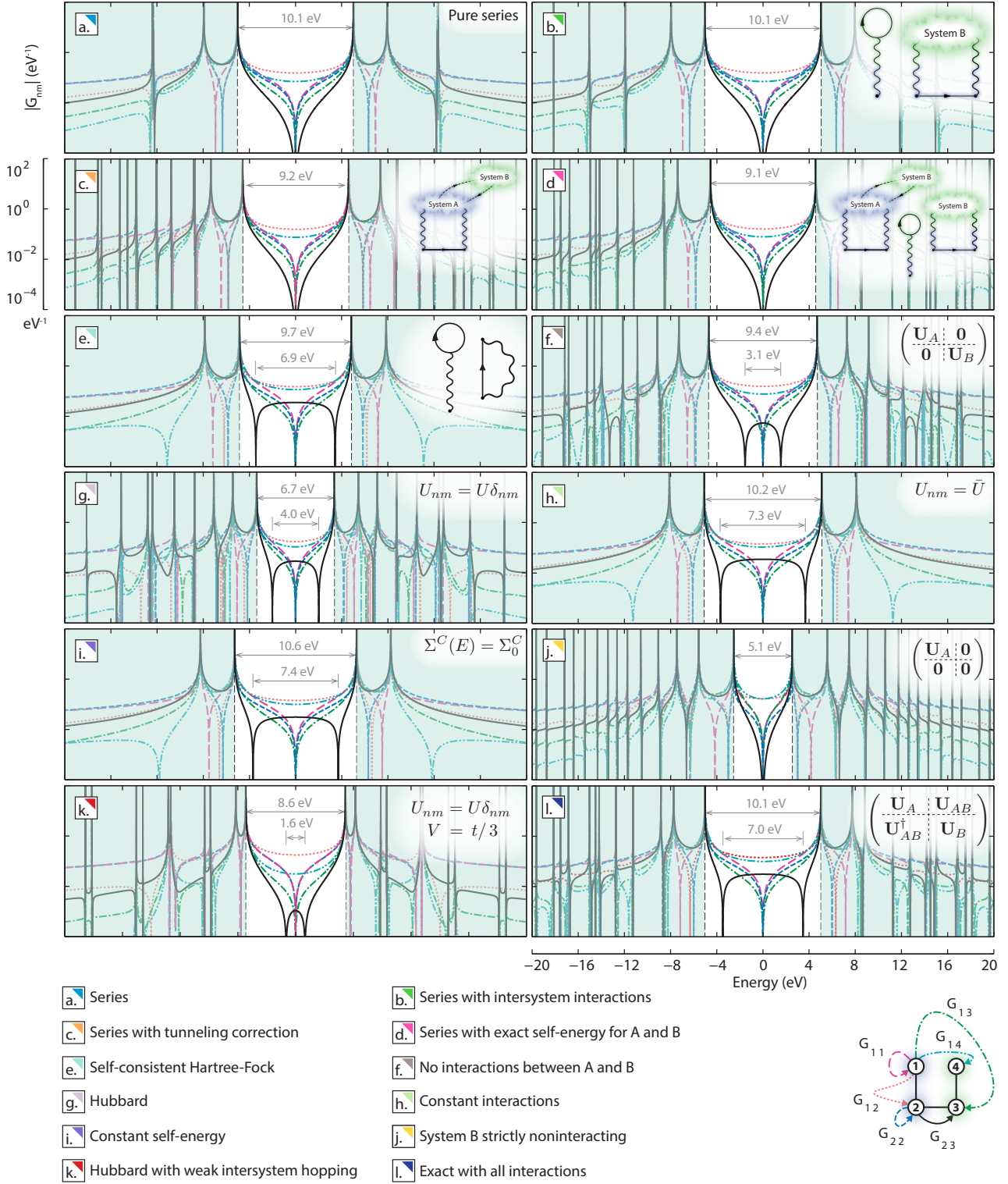


FIG. 9. The absolute elements of the retarded Green's function of system $A + B$ at half-filling, calculated via exact diagonalization. The calculation is performed with various parameterizations or in such a manner as to selectively include the processes depicted schematically in Figure 3. In this case, the presence of diagrams of the form (d) or (e) is necessary and sufficient to destroy the degenerate node in G_{23} . Other features in the low-energy region accessible to particles at the Fermi level (white) show no such sensitivity here.

of diagrams of the form (a) and (d), self-consistent Hartree-Fock calculations were performed to determine the Green's function of system $A + B$. The degenerate node is split, and calculations including only the Hartree diagram (not shown) indicate that the Fock diagram is responsible.

Thus nonlocal exchange is *sufficient* to split the degenerate node; however, it is not necessary or even the dominant contribution to the node splitting, as the remaining cases demonstrate.

f. No interactions between systems A and B: Here the Green's function of $A + B$ is calculated exactly with no interactions between A and B (i.e. $\mathbf{U}_{AB} = \mathbf{0}$). The degenerate node is split by roughly 3 eV and, on the basis of the foregoing cases and the fact that there are no intersystem interactions whatsoever, we conclude that diagrams of the form (e) are responsible.

g. Hubbard interactions: Here the Green's function of $A + B$ is calculated exactly with Hubbard interactions (i.e. $U_{nm} = \delta_{nm}U$). Again, a very large splitting is present despite no long-ranged interactions whatsoever. In light of the other cases, we conclude diagrams of the form (e) are responsible.

h. Constant interactions: As it is mentioned repeatedly in this work, we consider here the case of constant interactions, i.e. $U_{nm} = \bar{U}$ where \bar{U} is the average of the full interaction matrix from Eq. (A2). Again a large splitting is present in G_{23} .

i. Fixed Coulomb self-energy: As it is relevant elsewhere in this work, we present here the case wherein the Coulomb self-energy Σ^C is fixed to its value at $E = 0$. The splitting shown is attributable to the elements of the Coulomb self-energy that connect systems A and B . These are precisely the elements that arise from diagrams of the form (d) and (e), or amalgams thereof.

j. System B strictly noninteracting: Here system B is strictly noninteracting. Diagrams of the form (d) and (e) are not present in this scenario, and consistent with this the degenerate node survives.

k. Hubbard interactions with weak intersystem hopping: Here the Green's function for system $A + B$ is calculated with Hubbard interactions $U_{nm} = \delta_{nm}U$ and $V = t/3$ rather than $V = t$ as in the other cases. This scenario has the weakest overall coupling between the systems, and consistent with this, the smallest splitting of the degenerate node. However, the node splitting is still significant.

Figure 5. A degenerate node from fine-tuned interactions: Finally, we present an example of a degenerate node that exists within an interacting system despite the presence of diagrams that are inconsistent with series propagation. The cost is that instead of its existence being ensured by the geometry of the system, the degenerate node requires fine-tuning of, for example, an interaction matrix element. Moreover, this example also demonstrates that a perturbation can destroy a degenerate node by of lifting rather than splitting.

We consider the system $A + B$ with the parameter-

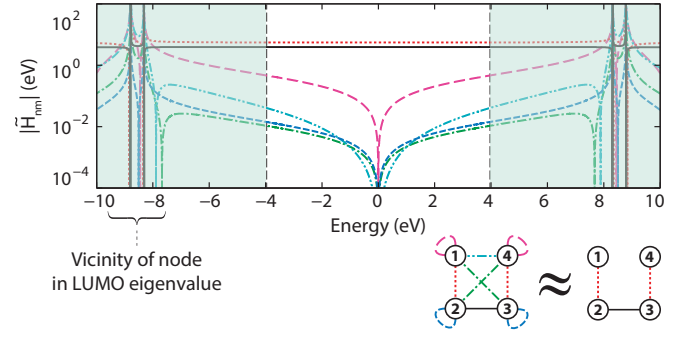


FIG. 10. The absolute matrix elements of the family of single-particle Hamiltonians defined by Eq. (A3). The parameters of the four-site extended Hubbard model are tuned such that $\tilde{H}_{14} \approx 0$ near $E = 0$. Since \tilde{H}_{11} , \tilde{H}_{22} , and \tilde{H}_{13} are suppressed at this point by particle-hole symmetry, the system has a “low-energy topology” that exhibits a degenerate node in the element G_{23} of the associated Green's function. This approximation breaks down near nodes in the eigenvalues of the Green's function (singularities in the self-energy), as can be seen around ± 8 eV.

ization given by $U = U_\alpha = U_\beta = 5$ eV, $U_\gamma = 0$ eV. In this case the supernode present within noninteracting models is not split, but completely lifted. This persists as $U_{14} = U_\gamma$ is increased, up to a critical value of ≈ 1 eV near which there is a sharp transition between the regimes of node lifting and splitting. At the critical value a supernode exists despite the presence of interactions that are inconsistent with series propagation, but at the cost of fine-tuning.

To investigate this phenomenon, it is instructive to use the exact Coulomb self-energy $\Sigma^C(E)$ to define a formal mapping of the many-body system $A + B$ onto a family of single-particle systems with Hamiltonians:

$$\tilde{H} = H_{A+B}^{(1)} + \Sigma^C(E) \quad (\text{A3})$$

where $H_{A+B}^{(1)}$ is the noninteracting portion of the Hamiltonian of system $A + B$. This reproduces the exact one-body Green's function by construction. The elements of \tilde{H} are plotted in Figure (10) for the critical value $U_\gamma = 0.969$ eV. Regardless of tuning, elements corresponding to next-next nearest neighbor hopping (e.g. Σ_{13}^C) break particle-hole symmetry and are therefore suppressed at half-filling near the particle-hole symmetric point ($E = 0$). At the critical value of U_γ , nonlocal exchange cancels exactly with higher order diagrams and the element Σ_{13}^C also vanishes, whereas for larger (smaller) values of U_γ it is respectively of the same or opposite sign as the hopping matrix elements in $H_{A+B}^{(1)}$. Thus, in this case, the competition between diagrams (d) and (e) leads to the switchover between node lifting and splitting depicted in Figure 5. Conclusive proof of the important qualitative role of higher order processes is furnished by self-consistent Hartree-Fock calculations (not shown), which do not lead to node lifting for this model.

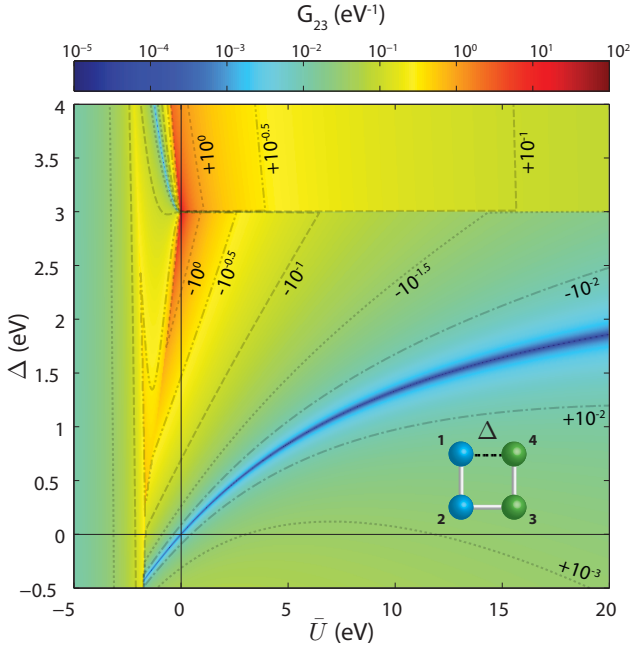


FIG. 11. The element G_{23} of the Green's function for system $A+B$ evaluated at the particle-hole symmetric point, plotted as a function of the average interaction matrix element \bar{U} and a hopping matrix element Δ connecting sites one and four. For simplicity, we have taken $V = t$ and constant interactions, i.e. $U_{nm} = \bar{U}$. A degenerate node exists for a family of parameterizations corresponding to the arc-shaped path that intersects $\bar{U} = 0$ eV, $\Delta = 0$ eV. However, it is forbidden by symmetry in the special case of $\Delta = t$. Absent the exact symmetry present in this case, the interplay between topology and interactions is complex.

As an aside, we note here that the approximate Hamiltonian obtained by setting $E = 0$ in the exact expression (A3) is valid only away from nodes in the eigenvalues of the Green's functions (singularities in the Coulomb self-energy).

Figure 11. A degenerate node from fine-tuning between a hopping matrix element and a charging energy \bar{U} with constant interactions: The generic dependence of degenerate nodes upon fine-tuning in the presence of interactions can be seen by considering the amplitude $G_{23}(E)$ evaluated at $E = 0$ as a function of parameters in the Hamiltonian. For simplicity, this is done in Figure 11 for system $A+B$ with all the interaction matrix elements set to a constant \bar{U} , with $V = t$, and a with a hopping matrix element Δ introduced between sites one and four. A degenerate supernode traces a path that corresponds to a family of models wherein $\tilde{H}_{14} = 0$. Just below this region the node is split, and above it, lifted.

The case $\Delta = t$ is also special in that symmetry then precludes the existence of a node at $E = 0$ regardless of the charging energy \bar{U} . This can be argued formally based on the eigenvectors of the Green's function, which here are just equal to the noninteracting ones. More generally, the same claim holds for non-constant interactions

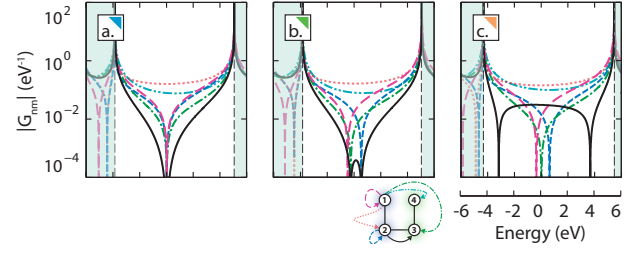


FIG. 12. The absolute elements of the retarded Green's function of a variation on the extended Hubbard system $A+B$, calculated at half-filling via exact diagonalization. Here the on-site energy of site 3 in system B is shifted up by 3 eV so that systems A and B are not identical and, moreover, there is no particle-hole symmetry. Panel (a) shows the results for pure series propagation (no diagrams from Figure 3), panel (b) shows the results with the inclusion of diagrams (a)-(c), and panel (c) shows the exact solution.

because in the presence of such symmetry, the interacting eigenvectors can be taken as equal to the noninteracting ones.

Figure 12. Broken symmetry between A and B : Up to this point we have only considered cases wherein systems A and B are identical. If this is not so, then it should perhaps not be surprising that a degenerate node expected on the basis of the alignment of nodes in A and B is disrupted. Figure 12 explores this, depicting the Green's function when the on-site potential of site 3 is shifted up by 3 eV:

Here panel (a) has only diagrams of the form (c), which, as before, do not perturb the node structure in $G^{A,B}$ (not shown) and therefore do not disrupt the nodes in G^{A+B} . Panel (b) has all diagrams of the form (a)-(c) and collectively these do split the degenerate node now. Since series propagation is enforced here, this must occur via a disruption of the relevant nodes in $G^{A,B}$. Moreover, to cause splitting these nodes must be shifted by different amounts, which requires that A and B be distinct. In this case it also necessitates broken particle-hole symmetry so that the nodes are not pinned at $E = 0$.

It is interesting to note, however, that diagrams (a)-(c) still only make a small contribution to the overall node splitting, as can be seen in panel (c), which shows the exact solution. Thus, at least in this case, the disruption of the degenerate node is not due primarily to changes in the electronic structure of A or B as defined by the dressing of $G^{A,B}$.

3. Greater than four sites

We discuss only briefly cases involving more than four sites. In particular, we consider an eight-site extended Hubbard model depicted in Figure 13 together with its node structure. Here the positions of local minima (dashed lines) and nodes (solid lines) in the element G_{27} of the retarded Green's function are shown as a function

of a dimensionless prefactor γ that premultiplies the interaction matrix U_{nm} . When this prefactor is unity, the parameters in the Hamiltonian are consistent with those for an organic molecule with the appropriate symmetry.

With $\gamma = 0$ this system exhibits a fourth order degenerate node where $G_{27} \propto E^4$. This splits into two local minima as interactions are introduced. As the strength of interactions passes some critical value γ_c these minima bifurcate and produce two lowest order nodes. Each of these three cases (i.e. $\gamma = 0$, $0 < \gamma < \gamma_c$, and $\gamma > \gamma_c$) can be understood in terms of the properties of the roots of the polynomial from Eq. (10).

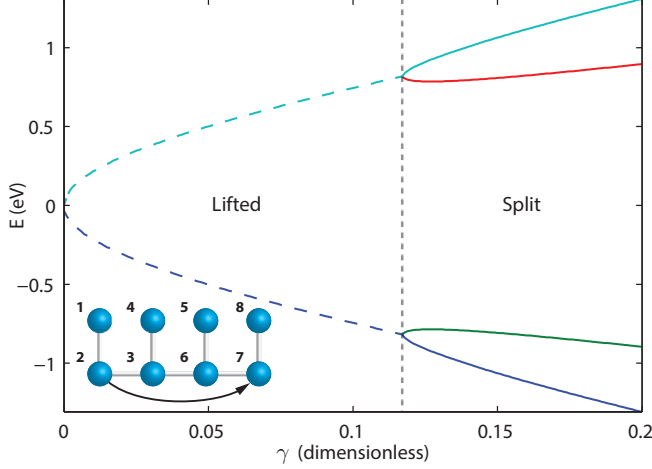


FIG. 13. The location of the nodes (solid lines) and minima (dashed lines) in the element G_{27} of the retarded Green's function associated with the depicted eight-site extended Hubbard system. Here γ is a dimensionless parameter that scales the strength of the interactions. The calculation was performed via exact diagonalization.

Appendix B: The connection between propagation and transmission

In section II we assumed little about the Green's function except that it vanishes when

$t < 0$. In particular, although the intuitive case of $G_{\beta\alpha}(t, 0) = -i\hbar\Theta(t)\langle d_\beta(t)d_\alpha^\dagger(0) \rangle$ was considered first to formulate a definition of series propagation, the preceding applies equally to the retarded Green's function³⁴ from the Keldysh formalism: $G_{\alpha\beta}(t, 0) = -i\hbar\Theta(t)\langle \{d_\beta(t), d_\alpha^\dagger(0)\} \rangle$. Transport related quantities are elegantly expressed via this quantity, as it combines the amplitudes for particle-like and hole-like processes, both of which contribute to e.g. charge and heat transport.

For a nanostructure wherein orbitals μ and ν are coupled to a metallic electrode via hopping matrix elements, the corresponding tunneling self-energy is of the form^{35,43} $\Sigma_{nm}^T = \Sigma_\mu^T \delta_{\mu n} \delta_{\mu m} + \Sigma_\nu^T \delta_{\nu n} \delta_{\nu m}$. Under these conditions the Dyson equation for the dressed retarded Green's function: \mathcal{G} :^{34,43}

$$\mathcal{G} = G + G\Sigma^T\mathcal{G}$$

implies:

$$\mathcal{G}_{\mu\nu} = \frac{G_{\mu\nu}}{(1 - G_{\mu\mu}\Sigma_\mu^T)(1 - G_{\nu\nu}\Sigma_\nu^T) - G_{\mu\nu}\Sigma_\nu^T G_{\nu\mu}\Sigma_\mu^T}. \quad (\text{B1})$$

Here we have assumed that the full self-energy associated with coupling is equal to the tunneling self-energy, i.e. taken the so-called elastic cotunneling approximation.^{8,36–38}

In the broad-band limit¹³ $\Sigma_\mu^T = -\frac{i\Gamma_\mu}{2}$ and $\Sigma_\nu^T = -\frac{i\Gamma_\nu}{2}$ in terms of elements Γ_μ and Γ_ν of a tunneling-width matrix. In this case the transmission function between the electrodes coupled to μ and ν is then given by:^{43,52–54}

$$T_{\mu\nu} = \Gamma^\mu \Gamma^\nu |\mathcal{G}_{\mu\nu}|^2 \propto G_{\mu\nu}$$

With regard to this work, the most important implication of the foregoing is that a node in $G_{\mu\nu}$ is sufficient for a node in $\mathcal{G}_{\mu\nu}$ and consequently $T_{\mu\nu}$.

Appendix C: A two-pole approximation for the eigenvalues of the retarded Green's function in extended Hubbard models

The retarded Green's function of an interacting system can be expressed in terms many-body energies and eigenstates via a Lehmann representation.^{8,35,55,56} In particular, at zero temperature:

$$G_{nm} = \underbrace{\frac{1}{\Omega_N} \sum_{\substack{\Psi \in \mathcal{B}_N^0 \\ \Psi' \in \mathcal{B}_{N+1}}} \frac{\langle \Psi | d_n | \Psi' \rangle \langle \Psi' | d_m^\dagger | \Psi \rangle}{E - [E_{\Psi'} - E_\Psi] + i0^+}}_{\text{Particle-like propagation}} + \underbrace{\frac{1}{\Omega_N} \sum_{\substack{\Psi \in \mathcal{B}_N^0 \\ \Psi' \in \mathcal{B}_{N-1}}} \frac{\langle \Psi | d_m^\dagger | \Psi' \rangle \langle \Psi' | d_n | \Psi \rangle}{E + [E_{\Psi'} - E_\Psi] + i0^+}}_{\text{Hole-like propagation}} \quad (\text{C1})$$

where $\mathcal{B}_N^0 = \{|\Psi\rangle\}$ is an orthonormal set of statistically occupied N particle ground states, $\mathcal{B}_{N\pm 1} = \{|\Psi'\rangle\}$ is an energy eigenbasis for the space of $N \pm 1$ particle states, and E_Ψ and $E_{\Psi'}$ are many-body energies. In the present context d_n^\dagger creates a particle on the n th spin-orbital in an extended Hubbard model, and Ω_N is the number of statistically accessible N particle ground states. For the sake of brevity, we consider the spin degrees of freedom to be implicit in the index n .

As an alternative to working in a localized basis, one can consider creation operators $d_\nu^\dagger(E)$ defined by:

$$d_n^\dagger = \sum_\nu \langle n|\nu\rangle d_\nu^\dagger(E) \quad (\text{C2})$$

or equivalently:

$$d_\nu^\dagger(E) = \sum_n \langle \nu|n\rangle d_n^\dagger \quad (\text{C3})$$

Here $\{|\nu(E)\rangle\}$ is an energy-dependent single-particle basis chosen to diagonalize the retarded Green's function, i.e. such that:

$$G = \sum_\nu \lambda_\nu |\nu\rangle \langle \nu| \quad (\text{C4})$$

where $\lambda_\nu(E)$ are the eigenvalues of G . This is always possible for an isolated system because the retarded Green's function is a normal matrix⁵⁷ in this case. Without loss of generality, we also assume that $\{|\nu(E)\rangle\}$ are eigenvectors of a set of generators for all the one-body symmetries of the system under consideration.

Formally, Eq. (C1) and the definition of $\{|\nu\rangle\}$ implies:

$$\lambda_\nu = \underbrace{\frac{1}{\Omega_N} \sum_{\substack{\Psi \in \mathcal{B}_N^0 \\ \Psi' \in \mathcal{B}_{N+1}}} \frac{\mathcal{Z}_\nu^{\Psi \rightarrow \Psi'}}{E - [E_{\Psi'} - E_\Psi] + i0^+}}_{\text{Particle-like propagation}} + \underbrace{\frac{1}{\Omega_N} \sum_{\substack{\Psi \in \mathcal{B}_N^0 \\ \Psi' \in \mathcal{B}_{N-1}}} \frac{\mathcal{Z}_\nu^{\Psi' \rightarrow \Psi}}{E + [E_{\Psi'} - E_\Psi] + i0^+}}_{\text{Hole-like propagation}} \quad (\text{C5})$$

where $\mathcal{Z}_\nu^{\Psi \rightarrow \Psi'} = |\langle \Psi'|d_\nu^\dagger|\Psi\rangle|^2$ are spectral weights associated with the transitions between many-body states. Since all $\Psi \in \mathcal{B}_N^0$ are associated with the same degenerate ground-state energy, this is equivalent to:

$$\lambda_\nu = \sum_{\Psi' \in \mathcal{B}_{N+1}} \frac{Z_\nu^{\Psi'}}{E - \varepsilon_\nu^{\Psi'} + i0^+} + \sum_{\Psi' \in \mathcal{B}_{N-1}} \frac{Z_\nu^{\Psi'}}{E + \varepsilon_\nu^{\Psi'} + i0^+} \quad (\text{C6})$$

where:

$$Z_\nu^{\Psi'} = \frac{1}{\Omega_N} \sum_{\Psi \in \mathcal{B}_N^0} \mathcal{Z}_\nu^{\Psi \rightarrow \Psi'} \quad (\text{C7})$$

and:

$$\varepsilon_\nu^{\Psi'} = E_{\Psi'} - E_\Psi \quad (\text{C8})$$

In the sum above, when Ψ' corresponds to a correlation-induced excited state, it contributes a narrow resonance at high-energy, e.g. in the shaded region inaccessible at the Fermi level in Figures 6 and 8. In the white regions in the same figures, these can be neglected or, as seen shortly, treated by renormalizing spectral weights. This suggests that, in the absence of orbital degeneracy, the eigenvalues λ_ν be approximated as:

$$\lambda_\nu \approx \frac{Z_\nu^p}{E - \varepsilon_\nu^p + i0^+} + \frac{Z_\nu^h}{E + \varepsilon_\nu^h + i0^+} \quad (\text{C9})$$

where:

$$Z_\nu^p = \frac{1}{\Omega_N} \sum_{\substack{\Psi \in \mathcal{B}_N^0 \\ \Psi' \in \mathcal{B}_{N+1}^0}} \mathcal{Z}_\nu^{\Psi \rightarrow \Psi'} \quad (\text{C10})$$

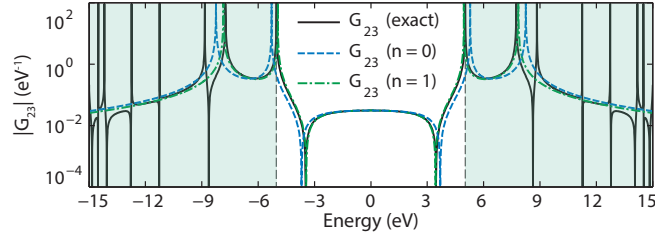


FIG. 14. The retarded Green's function of the four-site extended Hubbard model considered in section A calculated exactly or using zeroth or first order approximations for the eigenvalues of the Coulomb self-energy. The eigenvectors are evaluated with the energy fixed at $E = 0$. The linear approximation is essentially exact below $E \approx \pm 8$ eV, where the Coulomb self-energy becomes non-analytic due to a singularity associated with a node in an eigenvalue of G .

and:

$$Z_\nu^h = \frac{1}{\Omega_N} \sum_{\substack{\Psi \in \mathcal{B}_N^0 \\ \Psi' \in \mathcal{B}_{N-1}^0}} Z_\nu^{\Psi \rightarrow \Psi'} \quad (\text{C11})$$

Here, $\varepsilon_\nu^{\text{p,h}}$ are energies associated with the particle-like and hole-like transitions with nonzero spectral weight closest to the Fermi level. Due to our choice of $|\nu\rangle$, the foregoing is also valid in the presence of an orbital degeneracy if it is due to a symmetry not broken by interactions.

To explore the approximation described by Eq. (C9), it is useful to consider briefly the limit of constant interactions,⁵⁸ i.e. $U_{nm} = U$, in which case it is equivalent to its exact counterpart Eq. (C6). In this case the many-body states are Slater determinants and the eigenvectors $|\nu\rangle$ are just the noninteracting ones. The spectral weights $Z_\nu^{\Psi \rightarrow \Psi'}$ are then zero or unity depending the occupancy of the spin-orbital $|\nu\rangle$ in $|\Psi\rangle$ and $|\Psi'\rangle$. Likewise, the energies $\varepsilon_\nu^{\text{p,h}}$ are given exactly by $\varepsilon_\nu^{\text{p}} = \varepsilon_\nu + U([N - N_0] + \frac{1}{2})$ and $\varepsilon_\nu^{\text{h}} = -\varepsilon_\nu - U([N - N_0] - \frac{1}{2})$. There are therefore no correlation induced resonances at high-energies, and the resonances in Eq. (C9) for λ_ν correspond to the addition or removal of a particle from the single-particle state $|\nu\rangle$.

If distance-dependent interactions are dialed on, i.e. $U_{nm} = U \rightarrow U + \Delta U_{nm}$, the eigenvalues λ_ν in Eq. (C6) and potentially the eigenvectors $\{|\nu\rangle\}$ deviate from those with constant interactions. At low energies (e.g. the white region in Figures 6 and 8), this comes primarily from a shift in the positions of the dominant resonances, which correspond to those present with constant interactions, as well as a reduction of their spectral weights $Z_\nu^{\text{p,h}}$. The latter occurs as spectral weight is transferred to the correlation-induced resonances at high energy.

Overall, we find that in the simple cases considered herein, an expression of the form (C9) with “effective” parameters $\tilde{\varepsilon}_\nu^{\text{p,h}}$, $0 < \tilde{Z}_\nu^{\text{p,h}} < 1$, and $\tilde{U} > 0$ reproduces the low-energy Green's function with high accuracy. Moreover, with long-ranged interactions these parameters are typically near to their bare values. While this method is similar to two-pole approximations applied to the Hubbard model^{2,28}, it is expected to work best when the length scale of the interactions is larger than or comparable to the size of the system considered.

This approximation may also be cast in terms of the eigenvalues of the Coulomb self-energy Σ_ν , which, from the Dyson equation^{34,43}, are related to the eigenvalues above simply by:

$$\lambda_\nu = \frac{1}{E - \varepsilon_\nu - \Sigma_\nu} \quad (\text{C12})$$

where ε_ν are the noninteracting energies. Eq. (C9) then corresponds to a Laurent expansion of the Coulomb self-energy with the form:

$$\Sigma_\nu = c_{-1} (E - E_0)^{-1} + c_0 + c_1 (E - E_0) \quad (\text{C13})$$

If there is particle-hole symmetry so that $\tilde{Z}_\nu^{\text{p}} = \tilde{Z}_\nu^{\text{h}} \equiv \frac{1}{2}\tilde{Z}_\nu$, then $E_0 = \tilde{\varepsilon} + \tilde{U}[N - N_0]$, $c_{-1} = \tilde{Z}_\nu^{-1} \left(\frac{\tilde{U}}{2}\right)^2$, $c_0 = E_0 - \tilde{\varepsilon}_\nu$, and $c_1 = 1 - \tilde{Z}_\nu^{-1}$. Here N_0 is the number of sites in the extended Hubbard Hamiltonian. The residue is associated with the nodes in λ_ν and the linear term adjusts the spectral weight of the dominant resonances in λ_ν in a manner reminiscent of a Fermi liquid.²⁹

The assumption of particle-hole symmetry above is appropriate when $|\nu\rangle$ is expected to be half-filled. If, for example, $|\nu\rangle$ is instead expected to be completely empty, then $\tilde{Z}_\nu^{\text{h}} = 0$. In this case $E_0 = \tilde{\varepsilon}_\nu + \tilde{U}([N - N_0] + \frac{1}{2})$, $c_{-1} = 0$,

$c_0 = E_0 - \varepsilon_\nu$, and $c_1 = 1 - \tilde{Z}_\nu^{-1}$. In general, this approximation breaks down near correlation-induced nodes in the eigenvalue, which correspond to singularities in the exact Coulomb self-energy that render it non-analytic.

As a concrete example of the foregoing, we offer Figure 14, which shows the element G_{23} of the Green's function of system $A + B$ (Figure 7) with long-ranged Coulomb interactions as specified by Eq. (A2). This is calculated at half-filling using zeroth or first order approximations for the eigenvalues Σ_ν and with the eigenvectors $|\nu\rangle$ held constant. The linear ($n = 1$) approximation is excellent below $E \approx \pm 8$ eV, where the Coulomb self-energy becomes non-analytic due to a correlation-induced singularity in one of its eigenvalues. Equivalently, at this location there is a node in an eigenvalue of the Green's function.

-
- * barr@physics.arizona.edu
- ¹ J.P. Bergfield, G.C. Solomon, C.A. Stafford, and M.A. Ratner. Novel quantum interference effects in transport through molecular radicals. *Nano letters*, 11(7):2759–2764, 2011.
 - ² J. Hubbard. Electron correlations in narrow energy bands. *Proceedings of the Royal Society of London. Series A. Mathematical and Physical Sciences*, 276(1365):238–257, 1963.
 - ³ K. Ohno. Some remarks on the Pariser-Parr-Pople method. *Theor. Chim. Acta*, 2:219, 1964.
 - ⁴ C. W. M. Castleton and W. Barford. Screening and the quantitative pi-model description of the optical spectra and polarizations of phenyl based oligomers. *J. Chem. Phys.*, 117:3570–3582, 2002.
 - ⁵ J. D. Barr, C. A. Stafford, and J. P. Bergfield. Effective field theory of interacting pi-electrons. *Phys. Rev. B*, 86:115403, Sep 2012.
 - ⁶ B. Muralidharan, A. W. Ghosh, and S. Datta. Probing electronic excitations in molecular conduction. *Phys. Rev. B*, 73:155410, Apr 2006.
 - ⁷ Julián Rincón, K. Hallberg, A. A. Aligia, and S. Ramasesha. Quantum interference in coherent molecular conductance. *Phys. Rev. Lett.*, 103:266807, Dec 2009.
 - ⁸ J. P. Bergfield and C. A. Stafford. Many-body theory of electronic transport in single-molecule heterojunctions. *Phys. Rev. B*, 79:245125, Jun 2009.
 - ⁹ Justin P. Bergfield, Michelle A. Solis, and Charles A. Stafford. Giant thermoelectric effect from transmission supernodes. *ACS Nano*, 4(9):5314–5320, 2010.
 - ¹⁰ Dan Bohr, Peter Schmitteckert, and Peter Wölfle. Dmrg evaluation of the kubo formula conductance of strongly interacting quantum systems. *EPL (Europhysics Letters)*, 73(2):246, 2007.
 - ¹¹ Yigal Meir and Ned S. Wingreen. Landauer formula for the current through an interacting electron region. *Phys. Rev. Lett.*, 68:2512–2515, Apr 1992.
 - ¹² Yigal Meir, Ned S. Wingreen, and Patrick A. Lee. Transport through a strongly interacting electron system: Theory of periodic conductance oscillations. *Phys. Rev. Lett.*, 66:3048–3051, Jun 1991.
 - ¹³ Antti-Pekka Jauho, Ned S. Wingreen, and Yigal Meir. Time-dependent transport in interacting and noninteracting resonant-tunneling systems. *Phys. Rev. B*, 50:5528–5544, Aug 1994.
 - ¹⁴ P. Sautet and C. Joachim. Electronic interference produced by a benzene embedded in a polyacetylene chain. *Chemical Physics Letters*, 153(6):511 – 516, 1988.
 - ¹⁵ Cendrine Patoux, Christophe Coudret, Jean-Pierre Lauenay, Christian Joachim, and Andr Gourdon. Topological effects on intramolecular electron transfer via quantum interference. *Inorganic Chemistry*, 36(22):5037–5049, 1997.
 - ¹⁶ S. N. YALIRAKI and MARK A. RATNER. Interplay of topology and chemical stability on the electronic transport of molecular junctions. *Annals of the New York Academy of Sciences*, 960(1):153–162, 2002.
 - ¹⁷ R Stadler, S Ami, C Joachim, and M Forshaw. Integrating logic functions inside a single molecule. *Nanotechnology*, 15(4):S115, 2004.
 - ¹⁸ Derek Walter, Daniel Neuhauser, and Roi Baer. Quantum interference in polycyclic hydrocarbon molecular wires. *Chemical Physics*, 299(1):139 – 145, 2004.
 - ¹⁹ San-Huang Ke, Weitao Yang, and Harold U. Baranger. Quantum-interference-controlled molecular electronics. *Nano Letters*, 8(10):3257–3261, 2008. PMID: 18803424.
 - ²⁰ Gemma C. Solomon, David Q. Andrews, Richard P. Van Duyne, and Mark A. Ratner. Electron transport through conjugated molecules: When the system only tells part of the story. *ChemPhysChem*, 10(1):257–264, 2009.
 - ²¹ Thorsten Hansen, Gemma C. Solomon, David Q. Andrews, and Mark A. Ratner. Interfering pathways in benzene: An analytical treatment. *The Journal of Chemical Physics*, 131(19):194704, 2009.
 - ²² Aleksey A. Kocherzhenko, Ferdinand C. Grozema, and Laurens D. A. Siebbeles. Charge transfer through molecules with multiple pathways: Quantum interference and dephasing. *The Journal of Physical Chemistry C*, 114(17):7973–7979, 2010.
 - ²³ Marcel Mayor, Heiko B. Weber, Joachim Reichert, Mark Elbing, Carsten von Hnisch, Detlef Beckmann, and Matthias Fischer. Electric current through a molecular rod: relevance of the position of the anchor groups. *Angewandte Chemie International Edition*, 42(47):5834–5838, 2003.
 - ²⁴ Manabu Kiguchi, Hisao Nakamura, Yuuta Takahashi, Takuya Takahashi, and Tatsuhiro Ohto. Effect of anchoring group position on formation and conductance of a single disubstituted benzene molecule bridging Au electrodes: Change of conductive molecular orbital and electron pathway. *The Journal of Physical Chemistry C*, 114(50):22254–22261, 2010.
 - ²⁵ M. Mayor, H.B. Weber, J. Reichert, M. Elbing, C. von Hnisch, D. Beckmann, and M. Fischer. Electric current through a molecular rod: relevance of the position of the

- anchor groups. *Angewandte Chemie International Edition*, 42(47):5834–5838, 2003.
- ²⁶ G.C. Solomon, J.P. Bergfield, C.A. Stafford, and M.A. Ratner. When small terms matter: Coupled interference features in the transport properties of cross-conjugated molecules. *Beilstein Journal of Nanotechnology*, 2:862, 2011.
- ²⁷ After preparation of this manuscript, we became aware via private correspondence that J. Bergfield has recently observed node splitting within a Hubbard model of a molecular junction in unpublished work.
- ²⁸ Laura M. Roth. Electron correlation in narrow energy bands. i. the two-pole approximation in a narrow s band. *Phys. Rev.*, 184:451–459, Aug 1969.
- ²⁹ LD Landau. The theory of a fermi liquid. *Sov. Phys. JETP*, 3(6):920, 1957.
- ³⁰ P. W. Anderson. Localized magnetic states in metals. *Phys. Rev.*, 124:41–53, Oct 1961.
- ³¹ T.D. Stanescu, P. Phillips, and T.P. Choy. Theory of the luttinger surface in doped mott insulators. *Physical Review B*, 75(10):104503, 2007.
- ³² R. P. Feynman. Space-time approach to non-relativistic quantum mechanics. *Rev. Mod. Phys.*, 20:367–387, Apr 1948.
- ³³ F.J. Dyson. The s matrix in quantum electrodynamics. *Physical Review*, 75(11):1736, 1949.
- ³⁴ L.V. Keldysh. Diagram technique for nonequilibrium processes. *Zh. Eksp. Teor. Fiz*, 47(4):151–165, 1964.
- ³⁵ H. Haug and A.P. Jauho. *Quantum Kinetics in Transport and Optics of Semiconductors*. Springer Series in Solid-state Sciences, v. 123. Springer-Verlag Berlin Heidelberg, 2008.
- ³⁶ A. Groshev, T. Ivanov, and V. Valtchinov. Charging effects of a single quantum level in a box. *Phys. Rev. Lett.*, 66:1082–1085, Feb 1991.
- ³⁷ DV Averin and Yu V Nazarov. Virtual electron diffusion during quantum tunneling of the electric charge. *Physical review letters*, 65(19):2446–2449, 1990.
- ³⁸ Michael Pustilnik and Leonid Glazman. Kondo effect in quantum dots. *Journal of Physics: Condensed Matter*, 16(16):R513, 2004.
- ³⁹ JH Wilkinson. The evaluation of the zeros of ill-conditioned polynomials. part i. *Numerische Mathematik*, 1(1):150–166, 1959.
- ⁴⁰ Kimio Ohno. Some remarks on the pariser-parr-pople method. *Theoretical Chemistry Accounts: Theory, Computation, and Modeling (Theoretica Chimica Acta)*, 2:219–227, 1964. 10.1007/BF00528281.
- ⁴¹ C. W. M. Castleton and W. Barford. Screening and the quantitative pi-model description of the optical spectra and polarizations of phenyl based oligomers. *The Journal of Chemical Physics*, 117(8):3570–3582, 2002.
- ⁴² Room temperature calculations were carried out and yielded results visually indistinguishable from those presented here.
- ⁴³ S. Datta. *Electronic Transport in Mesoscopic Systems*. Cambridge Studies in Semiconductor Physics and Micro-electronic Engineering. Cambridge University Press, 1997.
- ⁴⁴ JM Luttinger. Fermi surface and some simple equilibrium properties of a system of interacting fermions. *Physical Review*, 119(4):1153, 1960.
- ⁴⁵ J. M. Luttinger and J. C. Ward. Ground-state energy of a many-fermion system. ii. *Phys. Rev.*, 118:1417–1427, Jun 1960.
- ⁴⁶ DV Averin and KK Likharev. Coulomb blockade of single-electron tunneling, and coherent oscillations in small tunnel junctions. *Journal of low temperature physics*, 62(3):345–373, 1986.
- ⁴⁷ T. A. Fulton and G. J. Dolan. Observation of single-electron charging effects in small tunnel junctions. *Phys. Rev. Lett.*, 59:109–112, Jul 1987.
- ⁴⁸ I. Giaever and H. R. Zeller. Superconductivity of small tin particles measured by tunneling. *Phys. Rev. Lett.*, 20:1504–1507, Jun 1968.
- ⁴⁹ H. R. Zeller and I. Giaever. Tunneling, zero-bias anomalies, and small superconductors. *Phys. Rev.*, 181:789–799, May 1969.
- ⁵⁰ More precisely, associated with the same eigenvalue of G ; the notion of a single-particle orbital here is formally justifiable when U_{nm} is constant.
- ⁵¹ To be precise, nonperturbative effects are included as well; therefore, in this context the diagrams mentioned should be viewed as a conceptual device used to classify processes. The only calculation performed diagrammatically was self-consistent Hartree-Fock.
- ⁵² Rolf Landauer. Spatial variation of currents and fields due to localized scatterers in metallic conduction. *IBM Journal of Research and Development*, 1(3):223–231, 1957.
- ⁵³ Rolf Landauer. Electrical resistance of disordered one-dimensional lattices. *Philosophical Magazine*, 21(172):863–867, 1970.
- ⁵⁴ Markus Büttiker. Absence of backscattering in the quantum hall effect in multiprobe conductors. *Physical Review B*, 38(14):9375, 1988.
- ⁵⁵ G. Kallen. On the definition of the renormalization constants in quantum electrodynamics. *Helvetica Physica Acta (Switzerland)*, 25, 1952.
- ⁵⁶ H. Lehmann, K. Symanzik, and W. Zimmermann. On the formulation of quantized field theoriesii. *Il Nuovo Cimento (1955-1965)*, 6(2):319–333, 1957.
- ⁵⁷ I.e. G commutes with its adjoint.
- ⁵⁸ Jürgen König, Herbert Schoeller, and Gerd Schön. Cotunneling at resonance for the single-electron transistor. *Phys. Rev. Lett.*, 78:4482–4485, Jun 1997.